



Article

Microstructure and Mechanical Properties of Core-Shell B₄C-Reinforced Ti Matrix Composites

Ziyang Xiu ^{1,*†}, Boyu Ju ^{1,*†} , Junhai Zhan ², Ningbo Zhang ³, Pengjun Wang ⁴, Keguang Zhao ⁵, Mingda Liu ⁶, Aiping Yin ², Weidi Chen ², Yang Jiao ², Hao Wang ², Shuyang Li ², Xiaolin Zhu ², Ping Wu ^{7,8,*} and Wenshu Yang ^{1,*} 

¹ State Key Laboratory of Advanced Welding and Joining, Harbin Institute of Technology, Harbin 150001, China

² Shanghai Aerospace System Engineering Research Institute, Shanghai 201108, China

³ Aerospace Research Institute of Materials & Processing Technology, Beijing 100076, China

⁴ Xi'an Honor Device Co., Ltd., Xi'an 710000, China

⁵ Huazhong Institute of Electro-Optics, Wuhan 430074, China

⁶ CASIC Space Engineering Development Co., Ltd., Xinzhou 431400, China

⁷ Key Laboratory of Advanced Science and Technology on High Power Microwave, Xi'an 710024, China

⁸ Northwest Institute of Nuclear Technology, Xi'an 710024, China

* Correspondence: xiuzy@hit.edu.cn (Z.X.); juboyu_hit@163.com (B.J.); wuping2007ssss@163.com (P.W.); yws001003@163.com (W.Y.)

† These authors contributed equally to this work.

Abstract: Composite material uses ceramic reinforcement to add to the metal matrix to obtain higher material properties. Structural design is an important direction of composite research. The reinforcement distribution of the core-shell structure has the unique advantages of strong continuity and uniform stress distribution. In this paper, a method of preparing boron carbide (B₄C)-coated titanium (Ti) powder particles by ball milling and preparing core-shell B₄C-reinforced Ti matrix composites by Spark Plasma Sintering was proposed. It can be seen that B₄C coated on the surface of the spherical Ti powder to form a shell structure, and B₄C had a certain continuity. Through X-ray diffraction characterization, it was found that B₄C reacted with Ti to form layered phases of titanium boride (TiB) and titanium carbide (TiC). The compressive strength of the composite reached 1529.1 MPa, while maintaining a compressive strain rate of 5%. At the same time, conductivity and thermal conductivity were also characterized. The preparation process of the core-shell structure composites proposed in this paper has high feasibility and universality, and it is expected to be applied to other ceramic reinforcements. This result provides a reference for the design, preparation and performance research of core-shell composite materials.

Keywords: B₄C; Ti matrix composite; core-shell composite; mechanical properties



Citation: Xiu, Z.; Ju, B.; Zhan, J.; Zhang, N.; Wang, P.; Zhao, K.; Liu, M.; Yin, A.; Chen, W.; Jiao, Y.; et al. Microstructure and Mechanical Properties of Core-Shell B₄C-Reinforced Ti Matrix Composites. *Materials* **2023**, *16*, 1166. <https://doi.org/10.3390/ma16031166>

Academic Editors: Sabina Lesz and Małgorzata Karolus

Received: 29 December 2022

Revised: 19 January 2023

Accepted: 29 January 2023

Published: 30 January 2023



Copyright: © 2023 by the authors. Licensee MDPI, Basel, Switzerland. This article is an open access article distributed under the terms and conditions of the Creative Commons Attribution (CC BY) license (<https://creativecommons.org/licenses/by/4.0/>).

1. Introduction

Compounding is an important material design method, which uses ceramic (such as SiC, B₄C, AlN, Si₃N₄, etc.) reinforcement to compound with a metal matrix to obtain higher material properties [1–3]. B₄C is an ideal reinforcement with a light weight, high hardness and high elastic modulus [4,5]. It is used in metal matrix composites to greatly improve the mechanical properties. Based on the excellent properties of B₄C, high-strength and high-wear resistant composites have been developed and applied in the military, automotive and nuclear industries [6,7].

The reinforcement of traditional B₄C/metal composites is mainly B₄C particles (B₄C_p). Researchers have carried out structural design research on B₄C_p/Al and B₄C_p/Ti matrix composites by adjusting the volume fraction, morphology and dispersion of B₄C. Luo and Zhang et al. [8,9] found that increasing the B₄C_p content could effectively improve

the properties, but when the mass fraction was 27.5%, B_4C_p agglomerated significantly, resulting in no further improvement in strength. Wu et al. [10] found that when the volume fraction was fixed, the smaller the B_4C_p diameter, the higher the strength. Small-size B_4C_p can effectively lead to larger values in strain gradient strengthening as well as CTE mismatch strengthening. Zhang et al. [11] prepared B_4C_p /TiAl composites with different mass fractions. It was found that the flexural strength and fracture toughness of 20 wt.% B_4C_p /TiAl were significantly improved compared with 10 wt.%. Selvakumar et al. [12] prepared 10 wt.% B_4C_p /Ti6Al4V composites and found that the hardness of the composites increased with the increase of the ball milling time. Chen et al. [13] prepared 30 wt.% B_4C_p /6061Al composites by hot pressing-extrusion-rolling. The high-volume fraction B_4C_p was uniformly dispersed, and the tensile strength of the composite reached 265 MPa. B_4C /Ti composites were prepared by a laser engineered net-shaping process by Nartu et al. [14], and the microscopic process of TiB and TiC formed by the reaction of B_4C and Ti was studied and analyzed.

A new study found that the powder with a core-shell structure has unique performance characteristics when sintered. The shell structure is connected into a network after sintering, which can effectively transfer the load and exert excellent mechanical properties. Yang et al. [15–17] oxidized Ti6Al4V titanium alloy powder at a high temperature to prepare a core-shell structure with the oxide of Ti6Al4V as the core and titanium as the shell. The titanium alloy powder with the core-shell structure was sintered into titanium matrix composites by spark plasma sintering. It was found that this structure has good oxidation resistance and high temperature stability. Li et al. [18] adsorbed B_4C on the surface of spherical Ti powder to prepare Ti- B_4C particles with a core-shell structure, and then reinforced 2024Al alloy. It was found that the yield strength of 10 wt.% Ti- B_4C /2024Al composites increased by 37.2% and the elongation increased by 6.3%. The excellent performance was attributed to the combined effect of the Ti particles, B_4C particles and in situ $TiAl_3$ phase. Zygula et al. [19] used B_4C to react with β -Ti alloy in situ to form TiB and TiC, and clarified the diffusion and reaction behavior of alloying elements. Jiang et al. [20] studied the reaction process of B_4C and Ti during SPS reaction. The products were mainly TiC, and a small amount of TiB and TiB_2 . However, the current research on B_4C /Ti composites is mostly focused on particle-reinforced metal matrix composites. The distribution of B_4C is dispersed, and there is no preparation method for core-shell B_4C /Ti composites. Furthermore, the effect of the shell-like distribution of B_4C on the properties of composites is not clear.

In this paper, Ti powder was used as the core and granular B_4C as the shell. The research on the preparation of composite materials with core-shell Ti- B_4C powder was carried out. The dispersion and preparation processes were optimized to guide the preparation of core-shell structural materials. The particularity of the core-shell structure and its unique mechanical properties were studied.

2. Materials and Methods

2.1. Raw Materials

The Ti powder used in this project was high-purity titanium powder, which was supplied by the Northwest Institute of Nonferrous Metals, China. In addition, its morphology was a spherical titanium powder with a larger particle size through plasma spheroidization. The energy spectrum analysis of the original spherical Ti powder was carried out. The experimental results are shown in Figure 1. It can be seen that the purity of Ti powder was high. Ti powder particle size distribution was in the range of 40–100 μm , and the shape in a better spherical, enlarged observation of its surface can be found on the surface of a smooth, not foreign matter, which also led to the powder having good fluidity. B_4C powders were supplied by Nangong Jingrui Alloy, China. The morphology of the original B_4C particles is shown in Figure 2. The average diameter of Ti powder used was 80 μm and that of B_4C powder was 10 μm .

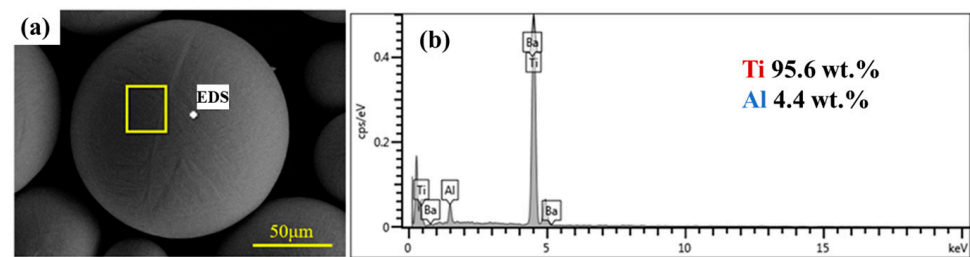


Figure 1. Raw material characterization of Ti powder. (a) Morphological characterization by SEM. (b) Element content characterization by EDS.

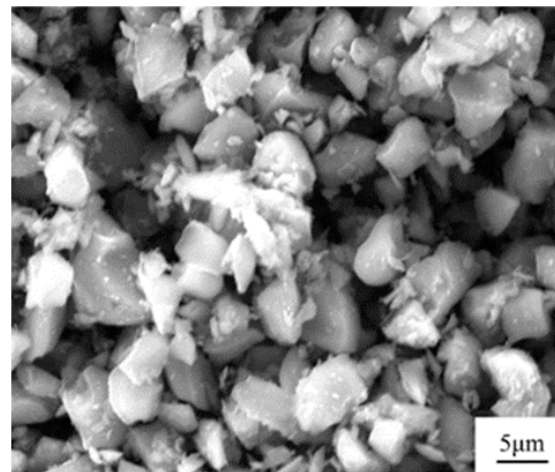


Figure 2. Raw material characterization of B₄C powder.

In this paper, the precursor particles (B₄C) were uniformly coated on the surface of the Ti powder by mechanical ball milling to form a core-shell structure of the B₄C precursor shell-coated Ti powder, as shown in Figure 3. B₄C coating on the surface of the Ti powder was achieved by mechanical ball milling. The volume fraction of B₄C was 30% in ball milling. The equipment used was the planetary ball mill apparatus QM-3SP2, from the Instrument Factory of Nanjing University, China. The mill and the ball used in the ball mill were both made of alumina. The diameter of the ball was 3 mm, and the volume of the ball mill was 500 mL. The rotation speed was 250 r/min, the ball milling time was 8 h and the ball milling atmosphere was ball milling under argon protection. The ball to material ratio was 5:1.

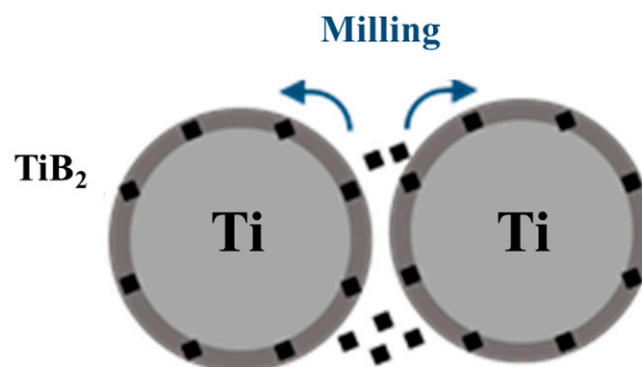


Figure 3. Preparation of core-shell Ti-B₄C composite by ball milling.

2.2. Preparation of Ti-Based Composites with a Core-Shell Microstructure

The core-shell structured powders were prepared by the Spark Plasma Sintering (SPS) process. SPS is a new material-sintering technology, which is widely used in the research and development of composite materials because of its fast-heating rate, short sintering time, controllable structure, energy saving and environmental protection [21,22]. After the powder coating process, 110 g mixed powder was stacked into high-density graphite die with an internal diameter of 50 mm. Then, sintering was performed on the SPS furnace (FCT HPD-250, Germany, Rauenstein) under a vacuum environment. For the sintering temperature, please reference the Ti alloy preparation temperature [23,24]. In this paper, the core-shell structure powder was continuously sintered at 1200 °C for 35 min. The sintering pressure, soaking time and vacuum were maintained at 40 MPa, 15 min and <8 Pa, respectively. After sintering, sintered composites were furnace-cooled to room temperature and the pressure was removed at 600 °C.

2.3. Microstructure Characterization of Ti-Based Composites

The phase composition of both the mixed powders and the composites were characterized by an Empyrean Intelligent X-ray Diffractometer (Malvern Panalytical, Malvern, UK). The specific test conditions were as follows: accelerating voltage 40 kV, current 40 mA, Cu-K α radiation, scanning speed 10°/min and scanning angle range 10~90°. Before the collection of the diffraction patterns, the tested powder was evenly and randomly laid on the glass test platform, and the surface of the tested composite block was sandpapered and cleaned with an acetone solution.

The microstructure of the mixed powder and the composites were observed and snapped by a ZEISS459315 (Carl Zeiss A.G., Oberkochen, Germany) metallographic microscope and Quanta 200FEG (FEI Company, Hillsboro, OR, USA) field-emission scanning electron microscopy (SEM) equipped with energy dispersive spectrometer (EDS). The sample with a dimension of 4 mm \times 5 mm \times 3 mm was obtained by electro discharge wire cutting. Before this, the observed samples were successively polished, cleaned and etched (400 #, 800 #, 2000 # and 4000 # sandpaper were selected for polishing, and a diamond polishing agent was selected for polishing cloth; the etched solution was Kroll reagent with a ratio of 20 vol%HF + 20 vol%HNO₃ + 60 vol%H₂O).

2.4. Performance Tests of Ti-Based Composites

2.4.1. Compression Test

The compression test was carried out on an Instron-8862 (Instron, Norwood, MA, USA) universal electronic testing machine with a constant displacement velocity of 0.25 mm/min for the indenter of the machine. To avoid defects from adversely affecting the compression test results, the test samples with a dimension of 4 mm \times 4 mm \times 6 mm were ground with 1500 # sandpaper until the surface had no obvious macroscopic defects. The compressive strength (P) of the composite could be estimated by:

$$P = \frac{F}{S} \quad (1)$$

where F is the maximum load when the specimen is fractured in compression and S denotes the cross-sectional area of the specimen perpendicular to the direction of the load. All samples were tested repeatedly more than five times to ensure the stability of the results.

2.4.2. Thermal Conductivity Measurement

The cylindrical specimen with the size of $\Phi 12.7$ mm \times 3.2 mm was processed by the wire-cutting method, and then the upper and lower surfaces of the specimen were polished with 1000 # sandpaper to ensure a smooth and flat surface. To ensure that the surface of the specimen was evenly heated during the thermal conductivity measurement, the upper and lower surfaces of the specimen were evenly coated with carbon powder after polishing. The thermal conductivity test experiments were performed on an LFA-447 laser

thermal conductivity meter manufactured by NETZSCH, which tests the thermal diffusion coefficient k of composite specimens at room temperature. The thermal conductivity λ of the composites could be obtained from:

$$\lambda = k \times \rho \times C \quad (2)$$

where k , ρ and C are the thermal diffusion coefficient, density and thermal capacity of the composites. ρ was obtained by Archimedes method and C was evaluated by the law of mixing.

3. Results and Discussion

3.1. Microstructure Characterization of Core-Shell Ti-B₄C Particles

Using the ball milling process parameters determined above, the large-sized spherical titanium powder and small-sized B₄C particles were ball milled to prepare a core-shell structure with spherical titanium powder as the core and B₄C as the shell. In order to prepare a thicker shell, the B₄C volume fraction was selected to be 30%. The surface morphology of the core-shell structure formed after ball milling is shown in Figure 4. It can be seen that the surface of the spherical titanium powder was obviously coated, but the uniformity was poor. The spherical titanium powder had a slight deformation in shape, but it was still spherical on the whole. After further magnification observation, compared with the original spherical titanium powder, it can be found that the spherical titanium powder particles were no longer smooth on the surface. Due to the high-volume fraction of the reinforcement precursor, some precursors were agglomerated on the surface, and many small particles were distributed on the surface.

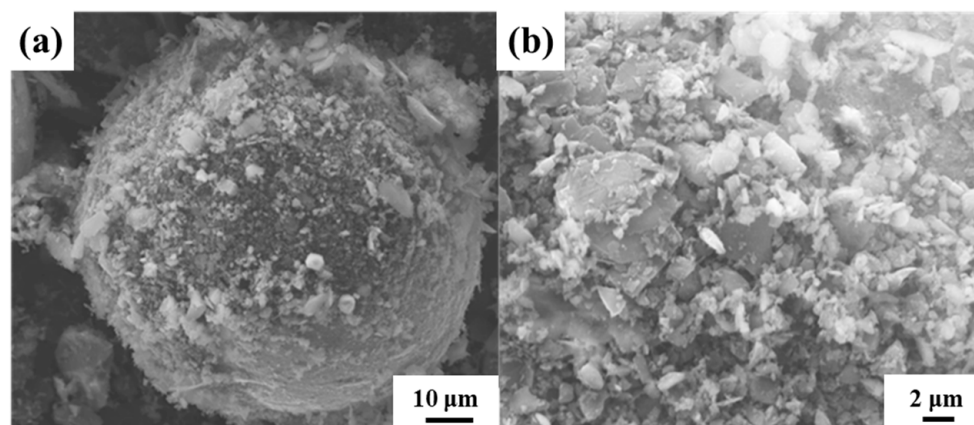


Figure 4. SEM characterization of core-shell Ti-B₄C (30 vol.%). (a) Core-shell Ti-B₄C, (b) the local amplification results of (a).

In order to analyze the composition distribution, the energy spectrum characterization of the core-shell structure Ti-B₄C was carried out, and the results are shown in Figure 5. It can be seen that the main component of the spherical particles was the Ti element, and a small amount of B and C elements were distributed on the surface, corresponding to the B₄C particles added by ball milling. It can be seen that B₄C particles were dispersed on the surface of the Ti powder after ball milling, forming the microstructure of B₄C-coated Ti. A discontinuous B₄C shell was formed on the surface of the Ti powder after sintering.

3.2. Microstructure Characterization of Ti-B₄C Composites

The Ti-B₄C core-shell structure was sintered by SPS with the parameters of 1200 °C –35 min and a preset pressure of 40 MPa. The metallographic structure is shown in Figure 6. The sintered composite formed a clear network structure, but there were obvious holes between the powder particles, and the density of the material was low. The composites were observed by SEM, as shown in Figure 7. It can be seen that the core-shell structure

unit based on the spherical Ti powder was retained, and the precursor particles coated with the spherical Ti powder formed a network reinforcement during the sintering process and bonded well with the matrix interface.

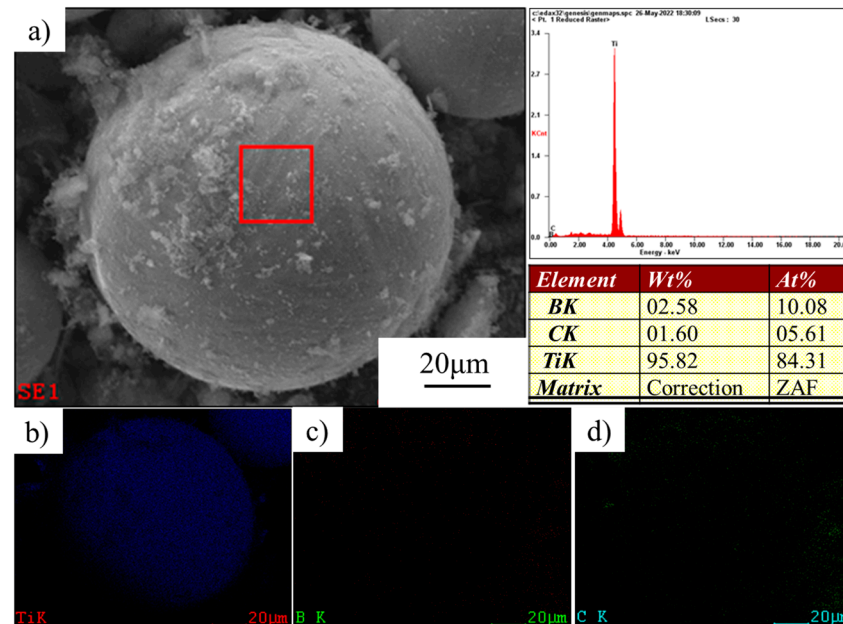


Figure 5. (a) EDS characterization of core-shell Ti-B₄C structure; (b–d) surface scanning analysis of Ti, B and C elements, respectively.

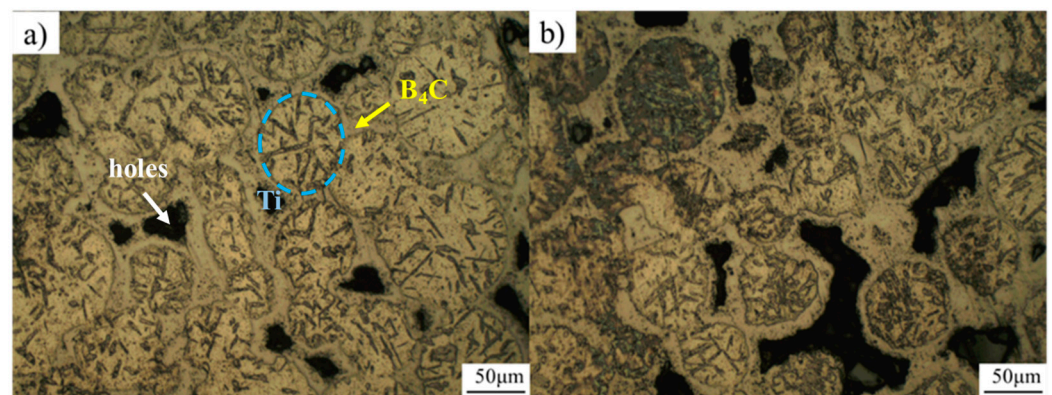


Figure 6. Metallographic characterization of Ti-B₄C composites; (a,b) are the representation of different regions.

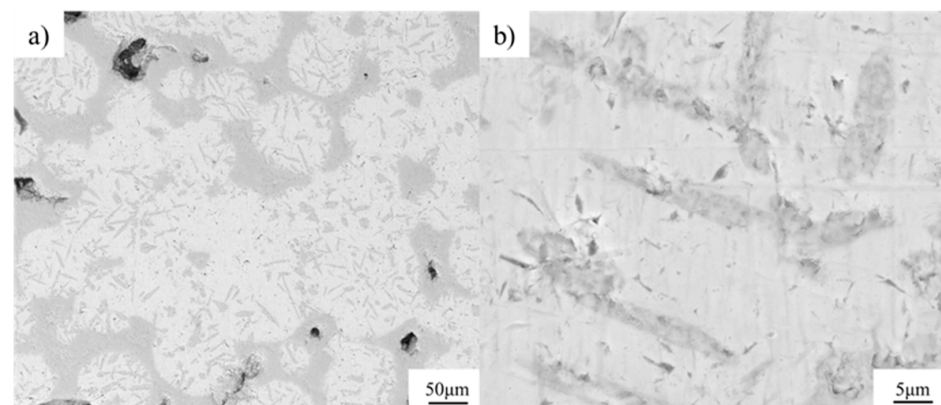


Figure 7. SEM backscattering of Ti-B₄C composites; (b) is the local amplification of (a).

The XRD phase compositions of the Ti-B₄C core-shell structure before sintering, after ball milling and the as-sintered composite were compared and analyzed. The results are shown in Figure 5. It can be seen that the reaction occurred during the ball milling process to generate TiB and TiC. After sintering, the phases were still dominated by Ti, B₄C, TiC and TiB, but the intensity of the characteristic peak of TiC increased, indicating that the interfacial reaction between B₄C and Ti further increased during sintering. A similar reaction process was found in the conventional particulate B₄C/Ti composites [14,25].

From the back-scattering characterization results of Figure 7, it can be seen that the Ti element was spherically distributed, while the light elements (B and C) were distributed on the surface of Ti, forming a shell structure. This structure was consistent with previous research results. The interfacial reaction between B₄C and Ti occurred, and a small amount of B₄C decomposed to form TiB and TiC, as shown in XRD (Figure 8). The needle-like TiB and TiC phase was distributed from the surface of Ti particles to the inside of the Ti particles. The B and C atoms provided by B₄C were diffused from the core-shell structure shell to the core, thus forming a staggered lamellar reinforcement inside the core-shell structure unit, and the results are shown in Figure 7.

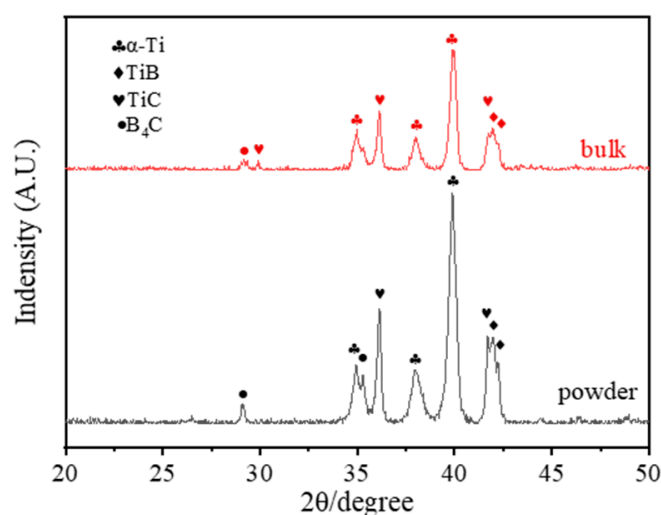


Figure 8. XRD characterization of Ti-B₄C core-shell structure powder and composite.

3.3. Mechanical and Functional Properties of Ti-B₄C Composites

The ability of a material to withstand axial static pressure at room temperature reflects the ability of the material to resist deformation during application, which depends on the type of reinforcement, interfacial bond strength, reinforcement distribution pattern and reinforcement content of the core-shell composite.

Figure 9 demonstrates the compressive stress–strain curves of the three core-shell structure composites B₄C/Ti. It can be seen that the plastic deformation phase was not obvious in the stress–strain curves of the three composites, which proves that the introduction of a large number of brittle reinforcements significantly increases the brittleness of the composites. For the B₄C/Ti composites, the interfacial reaction between B₄C and Ti produced TiB and TiC, forming a better interfacial bond. The good interfacial bonding strength resulted in the B₄C/Ti core-shell structure composite with a compressive strength of 1529.1 MPa. Compared to the compressive strength of the Ti matrix, the yield strength of all three composites was significantly improved. Typically, the B₄C/Ti composite has a 3.8-times improvement in the yield strength, as shown in Table 1.

Figure 10 shows the room-temperature compression fracture morphology of B₄C/Ti core-shell structure composites. It can be seen that the fractures' surfaces of B₄C/Ti composites were uneven, which suggest that the crack expansion path in the composite was increased, causing the composite to absorb more energy before the fracture. Therefore, the

compressive strain rate of more than 5% is still maintained at a high B_4C volume fraction (30 vol.%).

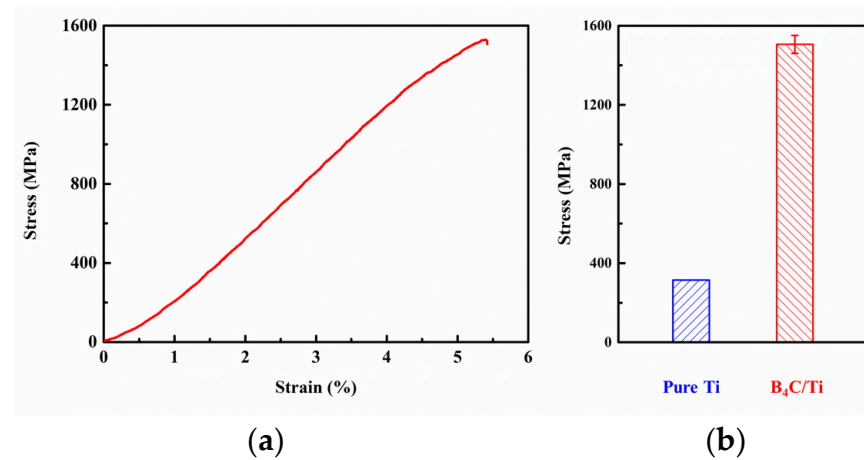


Figure 9. Compressive mechanical properties of composites with core-shell structure; (a) strain–stress curves; (b) comparison of mechanical properties (the yield strength of pure Ti is obtained from ref. [26]).

Table 1. The mechanical properties of B_4C/Ti composites were reported.

	Composite	Mechanical Properties
Zhang [11]	30 wt.% $B_4C/TiAl$	Bending 437.3 MPa
Yang [15,16]	(TiB, TiC, Nd_2O_3)/Ti	Bending 1150 MPa
Choi [25]	20 wt.% B_4C/Ti	Tensile 699 MPa
Wu [27]	Monolithic B_4C/Ti	Flexural 496.2 MPa
Han [28]	1 wt.% B_4C/Ti	Tensile 945 MPa
Li [29]	5 wt.% B_4C/Ti	Tensile 1126.1 MPa
This work	30 vol.% core-shell B_4C/Ti	Compressive 1529.1 MPa

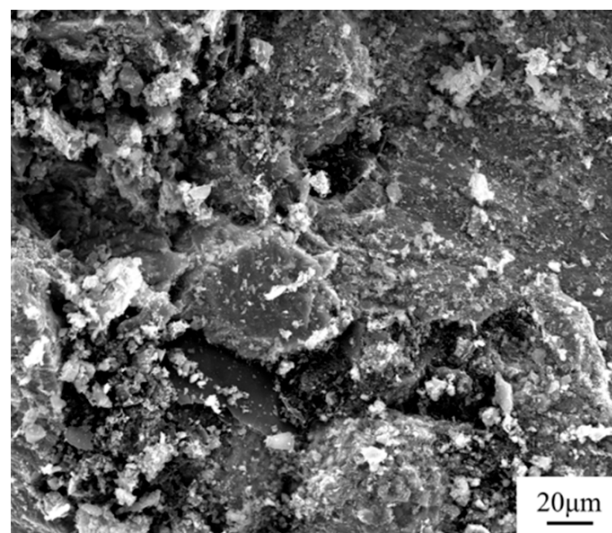


Figure 10. Fractured surface morphology of B_4C/Ti composites with core-shell structure.

In addition, the hardness, thermal conductivity and electric conductivity of the B_4C/Ti composites were tested, and the results are shown in Table 2. The hardness of the B_4C/Ti composites reached a high level (697.89 HV), which indicates that the B_4C reinforcement has a more favorable strengthening effect. At the same time, due to the influence of pores,

the electrical conductivity and thermal conductivity of the composites were low. The test results of this material provide a reference for subsequent core-shell material designs.

Table 2. Functional properties of B₄C/Ti composites.

Properties	B ₄ C/Ti	Ti
Density	4.32 g/cm ³	4.54 g/cm ³
Hardness	697.9 HV	210 HV
Thermal conductivity	13.0 W/m·K	14.6 W/m·K
Electric conductivity	0.64 Ω·mm ² /m	2.34 Ω·mm ² /m

4. Conclusions

In this paper, Ti-B₄C core-shell structure composites were prepared by ball milling and SPS. The mechanical properties, electrical conductivity and thermal conductivity of the composites were studied. B₄C reacts with Ti to form TiB and TiC, and obvious pores and defects are observed in the composites. The compressive strength of core-shell B₄C/Ti composites is up to 1529.1 MPa, which, compared with the Ti matrix, has a substantial increase, while the material maintains a compressive strain of 5%. This result has reference significance for the preparation of core-shell B₄C/Ti composites.

Author Contributions: Conceptualization, Z.X., B.J., P.W. (Pengjun Wang) and W.Y.; data curation, Z.X., J.Z. and K.Z.; formal analysis, J.Z., Y.J. and H.W.; funding acquisition, W.Y.; investigation, X.Z., K.Z., M.L. and S.L.; methodology, P.W. (Ping Wu); project administration, J.Z., A.Y., M.L. and W.C.; resources, B.J., W.C. and H.W.; supervision, X.Z., P.W. (Ping Wu) and S.L.; validation, S.L., A.Y. and W.C.; writing—original draft, Z.X., N.Z. and P.W. (Ping Wu); writing—review and editing, B.J., X.Z., P.W. (Pengjun Wang) and W.Y. All authors have read and agreed to the published version of the manuscript.

Funding: This work was financially supported by the National Key Research and Development Program of China (No. 2022YFE0121400), the National Natural Science Foundation of China (Grant Nos. 52171136, 51871072, 51871073), the Excellent Youth Scholars Project of Natural Science Foundation of Heilongjiang Province (YQ2021E016) and the Heilongjiang Touyan Team Program.

Institutional Review Board Statement: Not applicable.

Informed Consent Statement: Not applicable.

Data Availability Statement: The data presented in this study are available on request from the corresponding author.

Conflicts of Interest: The authors declare no conflict of interest.

References

- Chen, G.; Yang, W.; Dong, R.; Hussain, M.; Wu, G. Interfacial microstructure and its effect on thermal conductivity of SiCp/Cu composites. *Mater. Des.* **2014**, *63*, 109–114. [\[CrossRef\]](#)
- Dong, R.; Yang, W.; Wu, P.; Hussain, M.; Wu, G.; Jiang, L. High content SiC nanowires reinforced Al composite with high strength and plasticity. *Mater. Sci. Eng. A* **2015**, *630*, 8–12. [\[CrossRef\]](#)
- Xue, W.; Jiang, L.; Zhang, B.; Jing, D.; He, T.; Chen, G.; Xiu, Z.; Wu, G. Quantitative analysis of the effects of particle content and aging temperature on aging behavior in B₄C/6061Al composites. *Mater. Charact.* **2020**, *163*, 110305. [\[CrossRef\]](#)
- Trujillo-Vázquez, E.; Pech-Canul, M.I.; Guía-Tello, J.C.; Pech-Canul, M.A. Surface chemistry modification for elimination of hydrophilic Al₄C₃ in B₄C/Al composites. *Mater. Des.* **2016**, *89*, 94–101. [\[CrossRef\]](#)
- Xian, Y.; Pang, X.; He, S.; Wang, W.; Wang, X.; Zhang, P. Microstructure and Mechanical Properties of Al6061-31vol.% B₄C Composites Prepared by Hot Isostatic Pressing. *J. Mater. Eng. Perform.* **2015**, *24*, 4044–4053. [\[CrossRef\]](#)
- Nasr Isfahani, M.J.; Payami, F.; Asadabad, M.A.; Shokri, A.A. Investigation of the effect of boron carbide nanoparticles on the structural, electrical and mechanical properties of Al-B₄C nanocomposites. *J. Alloys Compd.* **2019**, *797*, 1348–1358. [\[CrossRef\]](#)
- Paidar, M.; Ojo, O.O.; Ezatpour, H.R.; Heidarzadeh, A. Influence of multi-pass FSP on the microstructure, mechanical properties and tribological characterization of Al/B₄C composite fabricated by accumulative roll bonding (ARB). *Surf. Coat. Technol.* **2019**, *361*, 159–169. [\[CrossRef\]](#)
- Luo, G.; Wu, J.; Xiong, S.; Shen, Q.; Wu, C.; Zhang, J.; Zhang, L. Microstructure and mechanical behavior of AA2024/B₄C composites with a network reinforcement architecture. *J. Alloys Compd.* **2017**, *701*, 554–561. [\[CrossRef\]](#)

9. Zhang, L.; Wang, Z.; Li, Q.; Wu, J.; Shi, G.; Qi, F.; Zhou, X. Microtopography and mechanical properties of vacuum hot pressing Al/B₄C composites. *Ceram. Int.* **2018**, *44*, 3048–3055. [\[CrossRef\]](#)
10. Wu, C.; Ma, K.; Wu, J.; Fang, P.; Luo, G.; Chen, F.; Shen, Q.; Zhang, L.; Schoenung, J.M.; Lavernia, E.J. Influence of particle size and spatial distribution of B₄C reinforcement on the microstructure and mechanical behavior of precipitation strengthened Al alloy matrix composites. *Mater. Sci. Eng. A* **2016**, *675*, 421–430. [\[CrossRef\]](#)
11. Zhang, W.; Gao, L.; Lei, Y.; Yang, B.; Li, J.; Xiao, L.; Yin, Y. TiAl/B₄C composite fabricated by high energy ball milling and hot press sintering processes and its mechanical properties. *Mater. Sci. Eng. A* **2010**, *527*, 7436–7441. [\[CrossRef\]](#)
12. Selvakumar, N.; Ramkumar, T. Effect of Particle Size of B₄C Reinforcement on Ti-6Al-4V Sintered Composite Prepared by Mechanical Milling Method. *Trans. Indian Ceram. Soc.* **2017**, *76*, 31–37. [\[CrossRef\]](#)
13. Chen, H.S.; Wang, W.X.; Nie, H.H.; Zhou, J.; Li, Y.L.; Liu, R.F.; Zhang, Y.Y.; Zhang, P. Microstructure evolution and mechanical properties of B₄C/6061Al neutron absorber composite sheets fabricated by powder metallurgy. *J. Alloys Compd.* **2018**, *730*, 342–351. [\[CrossRef\]](#)
14. Nartu, M.S.K.K.Y.; Mantri, S.A.; Pantawane, M.V.; Ho, Y.-H.; McWilliams, B.; Cho, K.; Dahotre, N.B.; Banerjee, R. In situ reactions during direct laser deposition of Ti-B₄C composites. *Scr. Mater.* **2020**, *183*, 28–32. [\[CrossRef\]](#)
15. Yang, Z.F.; Lu, W.J.; Xu, D.; Qin, J.N.; Zhang, D. In situ synthesis of hybrid and multiple-dimensioned titanium matrix composites. *J. Alloys Compd.* **2006**, *419*, 76–80. [\[CrossRef\]](#)
16. Yang, Z.F.; Lu, W.J.; Qin, J.N.; Gu, J.J.; Zhang, D.; Liu, J.L. Microstructural characterization of Nd₂O₃ in in situ synthesized multiple-reinforced (TiB+TiC+Nd₂O₃)/Ti composites. *J. Alloys Compd.* **2006**, *425*, 379–383. [\[CrossRef\]](#)
17. Yang, Z.; Lu, W.; Qin, J.; Zhang, D. Microstructure and tensile properties of in situ synthesized (TiC+TiB+Nd₂O₃)/Ti-alloy composites at elevated temperature. *Mater. Sci. Eng. A* **2006**, *425*, 185–191. [\[CrossRef\]](#)
18. Li, G.; Lyu, S.; Zheng, R.; Li, Q.; Ameyama, K.; Xiao, W.; Ma, C. Strengthening 2024Al alloy by novel core-shell structured Ti/B₄C composite particles. *Mater. Sci. Eng. A* **2019**, *755*, 231–234. [\[CrossRef\]](#)
19. Zyguła, K.; Wojtaszek, M. Processing and Characterization of beta Titanium Alloy Composite Using Power Metallurgy Approach. *Materials* **2022**, *15*, 5800. [\[CrossRef\]](#)
20. Jiang, D.; Cui, H.; Zhao, X.; Chen, H.; Ma, G.; Song, X. Reaction mechanism and friction behavior of an in-situ Ti/B₄C composite synthesized by spark plasma sintering. *Ceram. Int.* **2022**, *48*, 34341–34349. [\[CrossRef\]](#)
21. Wu, G.; Yu, Z.; Jiang, L.; Zhou, C.; Deng, G.; Deng, X.; Xiao, Y. A novel method for preparing graphene nanosheets/Al composites by accumulative extrusion-bonding process. *Carbon* **2019**, *152*, 932–945. [\[CrossRef\]](#)
22. Kang, P.; Zhao, Q.; Guo, S.; Xue, W.; Liu, H.; Chao, Z.; Jiang, L.; Wu, G. Optimisation of the spark plasma sintering process for high volume fraction SiCp/Al composites by orthogonal experimental design. *Ceram. Int.* **2021**, *47*, 3816–3825. [\[CrossRef\]](#)
23. Zhang, N.; Sun, D.; Han, X.; Wang, Z.; Liu, H.; Wang, Z.; Yang, W.; Wu, G. Effect of spark plasma sintering temperatures on microstructure and mechanical properties of in-situ (La₂O₃ + TiB)/Ti₂AlNb composites with a tailored three-dimensional network architecture. *Mater. Sci. Eng. A* **2020**, *772*, 138769. [\[CrossRef\]](#)
24. Wang, G.; Sui, X.; Liu, Q.; Liu, Y. Fabricating Ti₂AlNb sheet with high tensile strength and good ductility by hot packed rolling the spark plasma sintered pre-alloyed powder. *Mater. Sci. Eng. A* **2021**, *801*, 140392. [\[CrossRef\]](#)
25. Choi, B.-J.; Kim, Y.-J. In-Situ (TiB+TiC) particulate reinforced titanium matrix composites: Effect of B₄C size and content. *Met. Mater. Int.* **2013**, *19*, 1301–1307. [\[CrossRef\]](#)
26. Shang, C.; Liu, T.; Zhang, F.; Chen, F. Effect of Network Size on Mechanical Properties and Wear Resistance of Titanium/Nanodiamonds Nanocomposites with Network Architecture. *Compos. Commun.* **2020**, *19*, 74–81. [\[CrossRef\]](#)
27. Wu, C.; Li, Y.; Xie, S. Micro-structure, mechanical properties and comparison of monolithic and laminated Ti-B₄C composite with Al doped. *J. Alloys Compd.* **2018**, *733*, 1–7. [\[CrossRef\]](#)
28. Han, C.; Babicheva, R.; Chua, J.D.Q.; Ramamurty, U.; Tor, S.B.; Sun, C.-N.; Zhou, K. Microstructure and mechanical properties of (TiB+TiC)/Ti composites fabricated in situ via selective laser melting of Ti and B₄C powders. *Addit. Manuf.* **2020**, *36*, 101466. [\[CrossRef\]](#)
29. Li, R.; Yue, H.; Luo, S.; Zhang, F.; Sun, B. Microstructure and mechanical properties of in situ synthesized (TiB+TiC)-reinforced Ti₆Al₄V composites produced by directed energy deposition of Ti and B₄C powders. *Mater. Sci. Eng. A* **2023**, *864*, 144466. [\[CrossRef\]](#)

Disclaimer/Publisher's Note: The statements, opinions and data contained in all publications are solely those of the individual author(s) and contributor(s) and not of MDPI and/or the editor(s). MDPI and/or the editor(s) disclaim responsibility for any injury to people or property resulting from any ideas, methods, instructions or products referred to in the content.